Electron acceleration by wave turbulence in a magnetized plasma

Rigby, A., Cruz, F., Albertazzi, B., Bamford, R., Bell, A. R., Cross, J. E., Fraschetti, F., Graham, P., Hara, Y., Kozlowski, P. M., Kuramitsu, Y., Lamb, D. Q., Lebedev, S., Marques, J. R., Miniati, F., Morita, T., Oliver, M., Reville, B., Sakawa, Y., ... Gregori, G. (2018). Electron acceleration by wave turbulence in a magnetized plasma. *Nature Physics*, *14*(5), 475-479. https://doi.org/10.1038/s41567-018-0059-2

Published in:
Nature Physics

Document Version:
Peer reviewed version

Electron Acceleration by Wave Turbulence in a Magnetized Plasma

A. Rigby,[1] F. Cruz,[2] B. Albertazzi,[3] R. Bamford,[4] A. R. Bell,[1] J. E. Cross,[1] F. Fraschetti,[5] P. Graham,[6] Y. Hara,[7] P. M. Kozlowski,[1] Y. Kuramitsu,[7,8] D. Q. Lamb,[9] S. Lebedev,[10] J. R. Marques,[3] F. Miniati,[11] T. Morita,[7] M. Oliver,[1] B. Reville,[12] Y. Sakawa,[7] S. Sarkar,[1,13] C. Spindloe,[4] R. Trines,[4] P. Tzeferacos,[1,9] L. O. Silva,[2] R. Bingham,[4,14] M. Koenig,[3] and G. Gregori[1,9]

[1] *Department of Physics, University of Oxford, Parks Road, Oxford OX1 3PU, UK*
[2] *GoLP/Instituto de Plasmas e Fusão Nuclear, Instituto Superior Técnico, Universidade de Lisboa, 1049-001 Lisbon, Portugal*
[3] *Laboratoire pour l'Utilisation de Lasers Intenses, UMR7605, CNRS CEA, Université Paris VI Ecole Polytechnique, 91128 Palaiseau Cedex, France*
[4] *Rutherford Appleton Laboratory, Chilton, Didcot OX11 0QX, UK*
[5] *Departments of Planetary Sciences and Astronomy, University of Arizona, Tucson, AZ 85721, USA*
[6] *AWE, Aldermaston, Reading, West Berkshire RG7 4PR, UK*
[7] *Institute of Laser Engineering, Osaka University, 2-6 Yamadaoka, Suita, Osaka 565-0871, Japan*
[8] *Department of Physics, National Central University, Taoyuan 320, Taiwan*
[9] *Department of Astronomy and Astrophysics, University of Chicago, 5640 S. Ellis Ave, Chicago, IL 60637, USA*
[10] *Imperial College London, London, SW72AZ, UK*
[11] *Physics Department, Wolfgang-Pauli-Strasse 27, ETH-Zürich, CH-8093 Zürich, Switzerland*
[12] *School of Mathematics and Physics, Queens University Belfast, Belfast BT7 1NN, UK*
[13] *Niels Bohr Institute, Blegdamsvej 17, 2100, Copenhagen Ø, Denmark*
[14] *Department of Physics, University of Strathclyde, Glasgow G4 0NG, UK*

Astrophysical shocks are commonly revealed by the non-thermal emission of energetic electrons accelerated in-situ [1–3]. Strong shocks are expected to accelerate particles to very high energies [4–6], however, they require a source of particles with velocities fast enough to permit multiple shock crossings. Whilst the resulting diffusive shock acceleration [?] process can account for observations, the kinetic physics regulating the continuous injection of non-thermal particles is not well understood. Indeed, this injection problem is particularly acute for electrons, which rely on high frequency plasma fluctuations to raise them above the thermal pool [7, 8]. Here we show, using laboratory laser-produced shock experiments, that in the presence of a strong magnetic field, significant electron preheating is achieved. We demonstrate that the key mechanism in producing these energetic electrons is through the generation of lower-hybrid turbulence via shock-reflected ions. Our experimental results are analogous to many astrophysical systems, including the interaction of a comet with the Solar-wind [9], a setting where electron acceleration via lower-hybrid waves is possible.

Lower-hybrid waves occur in a variety of laboratory and space environments. They have been suggested to be an important electron-heating or energization mechanism in different magnetized plasma environments [10–12]. These waves propagate nearly transverse to the magnetic field lines and oscillate at a frequency between the ion gyro frequency and the electron gyro frequency. As a consequence lower-hybrid waves with frequency ω and wavenumber $\mathbf{k}$ can be in simultaneous Cerenkov resonance, $\omega - \mathbf{k}\cdot\mathbf{v} = 0$ (where $\mathbf{v}$ is the particle velocity) both with magnetized electrons propagating along the field lines and unmagnetized ions moving perpendicular to the field. The lower-hybrid waves have a high phase velocity along the field lines that resonate with the fast moving electrons as well as a low phase velocity across the field lines that resonate with the slow moving ions, allowing for energy transfer between the two species [13]. This convenient property of lower-hybrid waves, as an efficient channel for the acceleration of electrons above the thermal background, is well known in the magnetically confined fusion community [14] where it has been exploited with considerable efficacy in past experiments [15, 16]. Although a different mechanism is favoured in toroidal field configurations, for highly oblique shocks such as might be created in the Solar wind [9], supernova explosions [11], or during the formation of galaxy clusters [17], it is thought that the modified two-stream instability [13] driven by reflected ions from the shock front, excites broad-band lower-hybrid modes. By comparing theoretical and numerical predictions with the experimental data on the modified two-stream instability, it may be possible to develop robust scaling relations to apply to the fusion relevant parameters (see Supplementary Information for further discussion).

While electron acceleration by lower-hybrid waves in the Solar system has been inferred from satellite measurements [9, 18], laboratory experiments provide reproducible and controllable conditions that can be used not only as a means of supporting space observations, but also for validating multi-scale transport predictions from simulation codes [19]. Here we show the results from an experiment where a laser-produced plasma flow impacts on a magnetized sphere (see Figure 1). This mimics, for example, the interaction of the Solar-wind plasma with a comet [9], an environment where excess X-ray generation

by accelerated electrons has been observed. While both lower-hybrid turbulence and charge exchange processes [20] are possible explanations, our experimental results are compatible only with the former (see Supplementary Information).

The experiment was conducted at the LULI laser facility at École Polytechnique (France). Various diagnostics were implemented to probe the plasma before and after the interaction with the sphere (see Figure 2 for details).

Streaked optical pyrometry (SOP) shows the optical plasma emission streaked in time. SOP indicates that the plasma travels at a velocity of 70 km/s, implying the fluorine ions have a kinetic energy ~ 500 eV. The interferometry data shows that for the magnetized sphere, there is a bulk electron density of $\sim 10^{17}$ cm^{-3} upstream of the shock, rising to 10^{18} cm^{-3} downstream of the shock. Optical spectroscopy data gives a bulk plasma temperature of 3 ± 1 eV. The optical data indicates that the interaction of the plasma with the sphere is different for the magnetized and non-magnetized cases (see e.g., [21]). For the non-magnetized sphere, there is less pronounced plasma build up in front of the sphere. Near the axis of the flow and close to the surface of the sphere a shock with ~ 1 mm stand-off distance can be seen. In the magnetized case, the perpendicular field lines constrain the flow, making it more difficult for the plasma to fully flow around the sphere. Consequently, there is a larger pressure build up in front of the sphere, generating a shock at ~ 2.5 mm stand-off position, larger than that of the non-magnetized case. Balancing the ram pressure of the plasma flow with that of the compressed magnetic field gives an estimation for the expected stand-off distance in the magnetized case of ~ 1 mm, similar to the experimental value.

To further understand the flow dynamics and its interaction with the sphere, 2-dimensional radiation-magnetohydrodynamics (MHD) simulations were performed using the FLASH code (see Supplementary Information). The simulations agree qualitatively with experimental measurements, as shown in Figure 2, while providing additional estimates of bulk plasma properties.

The magnetic field carried by the ablated plasma is weak, and from the measured plasma parameters we infer the shock formed to be highly super-critical with a fast magneto-sonic Mach number of 5.7 ± 0.2, necessitating a significant reflected ion component [22].The electric field influencing the plasma near the shock can be estimated using the magnetic field and ion density calculated in FLASH (see Supplementary Information). For the shock to reflect incoming ions, the cross-shock electric potential must exceed the kinetic energy of the incoming ions. FLASH simulations predict an electric field of ~ 70 MeV/m at a distance of 0.5 mm from the sphere at 300 ns, increasing as the simulation progresses. Assuming a shock thickness on the order of the electron skin-depth $L \sim 10$ μm results in a cross-shock potential ≈ 700 eV, sufficient to reflect incoming Fluorine ions, with kinetic energy of ~ 500 eV. These reflected ions produce the counter-streaming ion flow, which are necessary for generating lower-hybrid turbulence, an effect not captured in FLASH simulations.

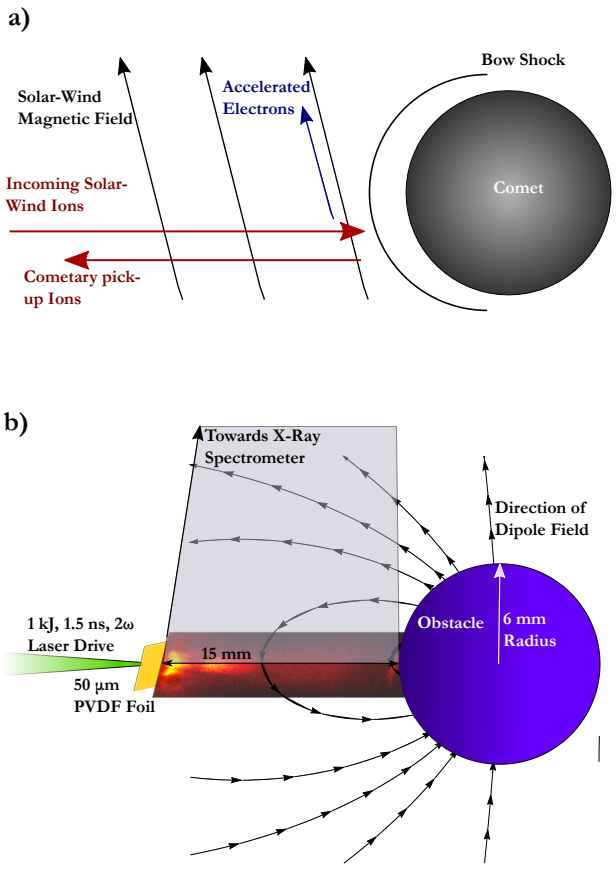

FIG. 1. **Illustration of a magnetized plasma-sphere interaction**. a) Interaction of a comet with the Solar-wind. The relative motion between the incoming Solar-wind ions and cometary pick-up ions, across the Solar-wind's magnetic field, result in the formation of the modified two-stream instability (MTSI) which, in turn, can excite waves within the lower-hybrid frequency range. The lower-hybrid waves can transfer energy from the counter-streaming ions traveling perpendicular to the magnetic field into accelerating electrons parallel to the magnetic field and so produce a suprathermal electron population. b) Schematic of the experimental setup. 1 kJ, 1.5 ns laser drive at 527 nm with a spot size of 200 μm diameter is impacted onto a 50 μm PVDF ($C_2H_2F_2$) foil target producing an expanding plasma jet from the back surface as shown in the overlaid image of the 550-800 nm optical emission of the plasma. A 12 mm diameter sphere is placed 15 mm from the target foil. The sphere is either a dipole magnetized Neodymium sphere with ≈ 7 kG surface field or a non-magnetized soda glass sphere of the same diameter. Optical diagnostics (interferometry and SOP) have ≈ 25 mm field of view, 250 ps gate time and look perpendicularly to the laser axis, similarly to the view above. An X-ray spectrometer spatially resolves along the laser axis with an RbAP crystal and spectrally resolves within the region of 630-770 eV.

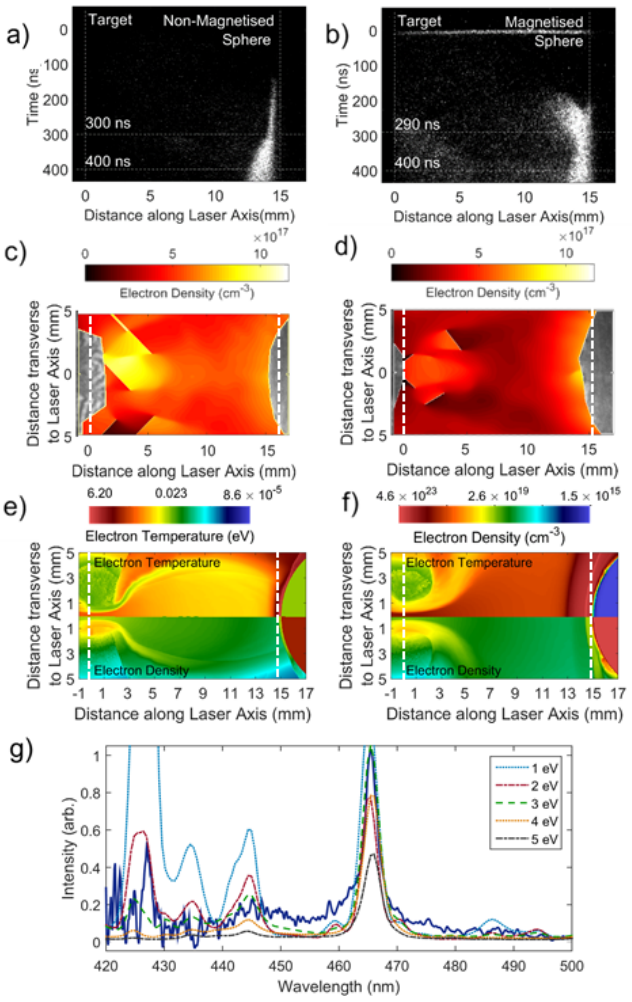

FIG. 2. **Optical Data and Radiation-hydrodynamic Simulations**. a) SOP data for a non-magnetized sphere. The plasma emission in the optical band 550-800 nm along the flow axis is streaked in time for 500 ns. Vertical dashed lines indicate the position of the target and sphere; horizontal lines indicate the time at which the interferometry data and FLASH simulation snapshot were taken. The plasma reaches the sphere in 200 ns indicating a flow velocity of 70 km/s. b) Same as a) but for a magnetized sphere. c) Transverse optical interferometry data taken at 300 ns for a non-magnetized sphere. The inferred electron density colour plot is overlaid (see Supplementary Information). d) Same as c) but taken at 290 ns for a magnetized sphere. e) Snapshot of a radiation-hydrodynamic simulation with no external field after 400 ns, symmetric about the laser-axis. Pseudocolour plots of electron temperature (top) and electron density (bottom) are shown. f) Same as e) but with a constant 5 kG field perpendicular to the flow axis. Colourbars are the same for both e) and f). g) Optical emission spectra of the plasma (dark blue solid line) at 300 ns, 12 mm from the target along the flow axis for the non-magnetized sphere case. Different spectra predicted by the code PrismSPECT (dashed lines) are overlaid and give a temperature best fit of 3 ± 1 eV (see Supplementary Information).

We have probed the plasma emission in the soft X-ray range (630-770 eV) with an X-ray spectrometer that spatially resolved along the flow axis (see Supplementary Information). The integrated intensity of the observed Fluorine X-ray line can then be plotted as a function of position along the flow axis (see Figure 3). When the magnetized sphere is present an excess in X-ray intensity is observed close to the sphere compared with the non-magnetized sphere. This excess in soft X-rays suggests that electrons of energies significantly greater than 3 eV must be present. As lower-hybrid turbulence requires the reflected ions to move perpendicularly to the field lines, we have have also considered the case when the sphere was rotated to have the magnetic dipole moment aligned with the flow, mimicking a parallel field line configuration. In the latter configuration, we found no appreciable increase in X-ray intensity close to the sphere relative to the non-magnetized case.

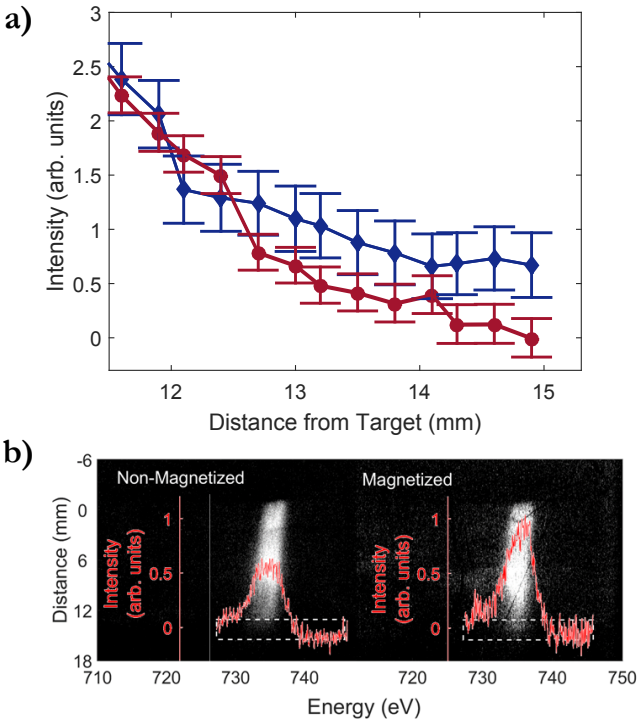

FIG. 3. **X-ray data**. a) Integrated X-ray intensity of the Fluorine He-α line as a function of position along the laser axis. Data for magnetized sphere shots (blue diamonds) has an increased intensity close to the sphere when compared with data for non-magnetized sphere shots (red circles). b) Normalized X-ray signal, showing the Fluorine He-α line for the non-magnetized (left) and magnetized (right) shots. For both cases, a white rectangle and an additional plot have been overlaid. The white rectangle indicates the region where the spatial lineouts were taken. The overlaid plots show the average spatially-integrated spectral line shape within the white rectangle (i.e. close to the sphere). The normalization for all the X-ray data has been chosen such that the peak intensity of the spectral line shape for the magnetized sphere in case b) is set to unity.

To investigate further the lower-hybrid origin for the excess X-ray emission near the magnetized sphere and the possible presence of a suprathermal electron population, we have performed 2D particle-in-cell (PIC) simulations of the plasma flow collision with the dipolar magnetic object (see Figure 4) using the massively parallel, fully relativistic code OSIRIS (see Supplementary Information).

OSIRIS simulation results indicate, in agreement with our previous FLASH simulations, that as the plasma impacts the sphere (of typical size larger than the ion Larmor radius), a bow shock develops [23]. The counter-propagating ion flow is unstable and excites plasma waves in the lower-hybrid range ahead of the shock front (see Figure 4). These waves are then amplified and break, resulting in a turbulent, compressed plasma region. In fact the ratio between the parallel ($k_\parallel$) and perpendicular ($k_\perp$) wavenumber of these modes is consistent with the idealised dispersion relation for lower-hybrid waves of $\frac{k_\parallel}{k_\perp} \approx \sqrt{\frac{m_e}{m_i}}$ [9], as highlighted in Figure 4 (m_e and m_i are the electron and ion masses, respectively). OSIRIS simulations also show that when crossing the shock, the upstream plasma is significantly heated The observed downstream wave spectrum is thus consistent with the hypothesis of a resonant interaction between electrons and ions being driven by lower-hybrid turbulence.

While the OSIRIS simulation indicates a significant heating of the plasma, because of finite computational resources, these are performed with an electron-ion mass ratio and plasma velocity different from that of the experiment. Thus, to apply the OSIRIS results to the measured data, the simulation conditions need to be properly re-scaled to those occurring in the experiment. The average energy of electrons accelerated by lower-hybrid waves can be estimated [9] by

$$E_e = \alpha^{2/5} \left(\frac{m_e}{m_i}\right)^{1/5} m_i u^2, \tag{1}$$

where α is an efficiency factor on the order of a few percent and u is the ion velocity (see Supplementary Information). Since OSIRIS simulations predict that lower-hybrid turbulence heats electrons to $E_e^{PIC} \sim 75$ keV, the rescaling to the laboratory conditions immediately follows from Equation 1:

$$\frac{E_e^{\mathrm{Lab}}}{45\ \mathrm{eV}} = \frac{E_e^{\mathrm{PIC}}}{75\ \mathrm{keV}} \left(\frac{m_e^{\mathrm{Lab}}}{m_e^{\mathrm{PIC}}}\right)^{1/5} \left(\frac{m_i^{\mathrm{Lab}}}{m_i^{\mathrm{PIC}}}\right)^{4/5} \left(\frac{u^{\mathrm{Lab}}}{u^{\mathrm{PIC}}}\right)^{2}, \tag{2}$$

where we have assumed the same efficiency factor both in the laboratory and in OSIRIS simulations. For the predicted average electron heating in the laboratory is $\sim$ 45 eV, this electron energy can then be used in Equation 1 to determine an efficiency factor of $\alpha \sim 0.1$. Our OSIRIS simulation suggests that these accelerated electrons have a nearly Gaussian spectrum. The high energy tail of this distribution is then responsible for the observed X-ray excess.

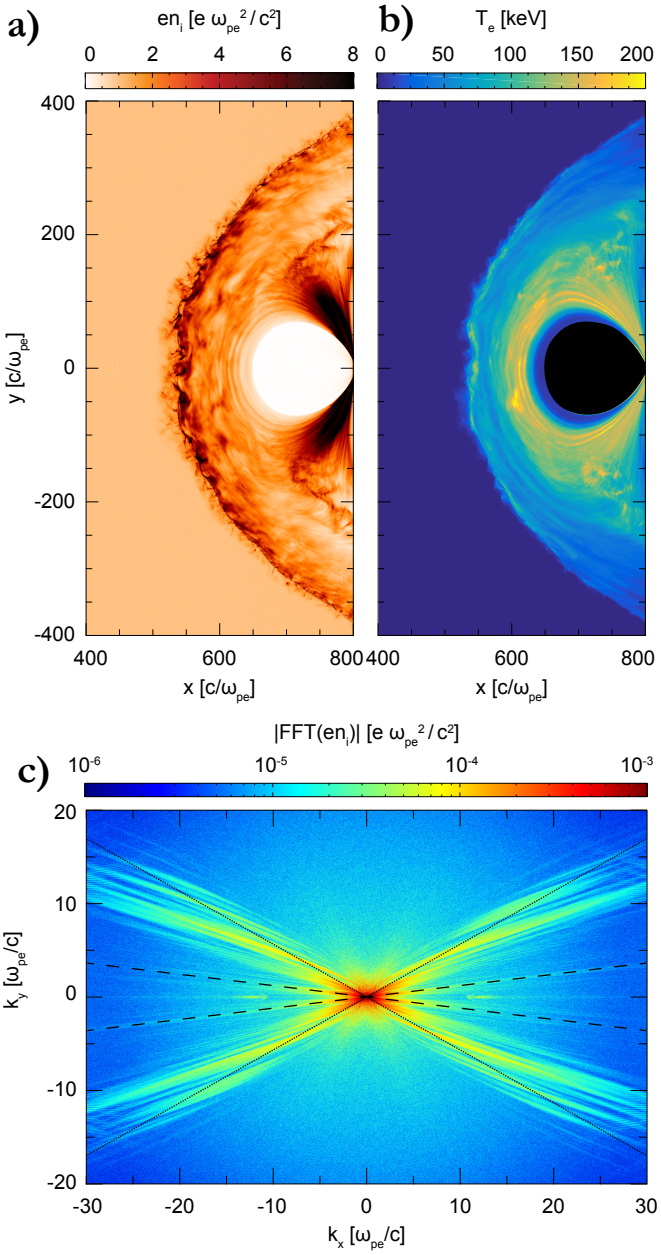

FIG. 4. **OSIRIS PIC Simulations**. a) injected ion density, b) electron temperature and c) wave spectrum. The wave spectrum is calculated by performing a Fourier transform on the ion density to gain information on the parallel and perpendicular k-numbers. The black dashed lines indicate modes that have a ratio in k-number consistent with the lower-hybrid dispersion relation for ions reflected horizontally off of the shock. The black dotted lines indicate modes that have a ratio in k-number consistent with the lower-hybrid dispersion relation for ions reflected on the flanks of the bow shock. All figures are taken at the same time of 6 ion cyclotron periods.

The collisional-radiative code PrismSPECT was used to calculate the X-ray emission from the predicted hot electron population of lower-hybrid electrons (see Supplementary Information). When no hot population was

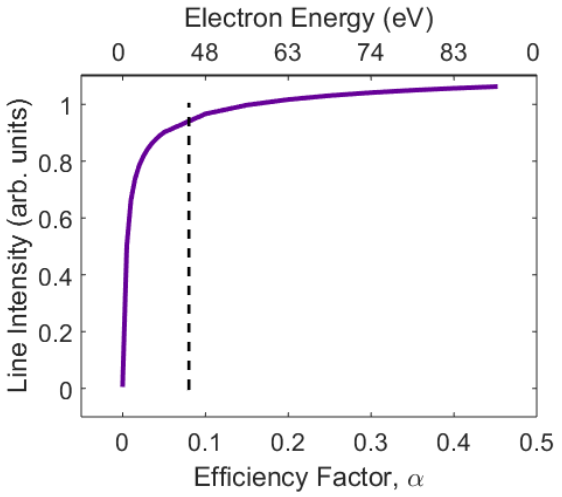

FIG. 5. **Atomic transition simulations**. Results from PrismSPECT (purple line) indicate that as the hot electron population is increased in both fraction and average energy according to the efficiency factor α from Equation 1, the logged intensity of the Fluorine He-α line also increases (the average electron energy for a given value of α is shown in the top horizontal axis for reference). When no hot electron population is present, no Fluorine He-α line is generated. There is minimal contribution from bremsstrahlung. The average hot electron energy ($E_e \sim 45$ eV) and efficiency factor ($\alpha \sim 0.1$) for laboratory conditions is indicated with the black dashed line.

present, no Fluorine X-rays were obtained. As the efficiency factor α increases, the X-ray intensity of the observed Fluorine line also increases (See Figure 5). The PrismSPECT results show that an average hot electron energy of at least 30 eV is sufficient to produce the X-rays observed within the laboratory.

In the experiment, the counter-streaming Fluorine ions have a collisional mean-free-path of ~ 5 mm (See Supplementary Information), to be compared with their gyroradius ~ 2 cm. This does not affect the growth of the lower-hybrid instability [13].

Our results provide compelling evidence that lower-hybrid waves play an important role in energizing electrons and thus provide a potential mechanism for overcoming the injection problem for perpendicular shocks. We infer the presence of this electron energization by the observation of excess X-ray emission from the plasma when a magnetized sphere is present. The magnetized sphere permits the generation of lower-hybrid waves through a shock-reflected ion instability, thus allowing these waves to energize the electrons by energy transfer from the ionic motion. Whilst this electron energization process has been inferred in many astrophysical environments, it is not fully understood and so makes our experiment an important platform for the validation of the particle acceleration models frequently invoked to explain the high energy electrons observed at strong astrophysical shocks.

[1] K. Koyama et al. *Evidence for shock acceleration of high-energy electrons in the supernova remnant SN1006*, Nature 378, 255–258, 1995

[2] A. Masters et al. *Electron acceleration to relativistic energies at a strong quasi-parallel shock wave*, Nature Physics 9, 164–167, 2013

[3] E. A. Helder et al. *Observational Signatures of Particle Acceleration in Supernova Remnants*, Space Science Reviews 173, 369-431, 2012

[4] R. Blandford and D. Eichler *Particle acceleration at astrophysical shocks: A theory of cosmic ray origin*, Physics Reports 154, 1, 1987

[5] R. Van Weeren et al. *Particle Acceleration on Megaparsec Scales in a Merging Galaxy Cluster*, Science 330, 347–349, 2010.

[6] A. Marcowith et al. *The microphysics of collisionless shock waves*, Reports on Progress in Physics 79, 046901, 2016

[7] T. Amano and M. Hoshino *Electron Injection at High Mach Number Quasi-perpendicular Shocks: Surfing and Drift Acceleration*, The Astrophysical Journal 661, 190–202, 2007

[8] M. Riquelme and A. Spitkovsky *Electron injection by Whistler waves in non-relativistic shocks*, The Astrophysical Journal 733, 63, 2011

[9] R. Bingham et al. *Generation of X-rays from Comet C/Hyakutake 1996 B2*, Science 275, 49–51, 1997

[10] K. G. McClements et al. *Acceleration of cosmic ray electrons by ion-excited waves at quasiperpendicular shocks*, Monthly Notices of the Royal Astronomical Society 291, 241–249, 1997

[11] R. Bingham et al. *X-ray emission from comets, cometary knots and supernova remnants*, The Astrophysical Journal 127, 233–237, 2000

[12] J. Vink and M. J. Laming *On the Magnetic Fields and Particle Acceleration in Cassiopeia A*, The Astrophysical Journal 584, 758-769, 2003

[13] J. B. McBride et. al. *Theory and Simulation of Turbulent heating by the Modified Two-Stream Instability*, Physics of Fluids 15, 2367, 1972

[14] N. J. Fisch. *Theory of Current Drive in Plasmas*, Reviews of Modern Physics, Volume 59, 1987

[15] M. Porkolab et al. *High-Power Electron Landau-Heating Experiments in the Lower Hybrid Frequency Range in a Tokamak Plasma*, Physical Review Letters, 53, 1229, 1984

[16] R. Cesario et al. *Current drive at plasma densities required for thermonuclear reactors*, Nature Comms. 1 (5), 55, 2010

[17] J. A. Eilek and J. C. Weatherall in *Diffuse thermal and relativistic plasma in galaxy clusters.* Edited by Hans Bohringer, Luigina Feretti, Peter Schuecker. Garching, Germany: Max-Planck-Institut fur Extraterrestrische Physik, p. 249, 1999

[18] I. H. Cairns and G. P. Zank *Turn-on of 2-3 kHz radiation beyond the heliopause*, Geophysical Research Letter 29,

1143, 2002

[19] Y. P. Zakharov et al. *Simulation of astrophysical plasma dynamics in the laser experiments*, AIP Conference Proceedings 369, 357–362, 2008

[20] P. Beiersdorfer et al. *Laboratory Simulation of Charge Exchange-Produced X-ray Emission from Comets*, Science 300, 1558–1559, 2003

[21] A. R. Bell et al. *Collisionless shock in a laser-produced ablating plasma*, Physical Review A 38, 1363, 1988

[22] R. Z. Sagdeev, *Cooperative phenomena and shock waves in collisionless plasmas*, Reviews of plasma physics 4, 23, 1966

[23] F. Cruz et al. *Formation of collisionless shocks in magnetized plasma interaction with kinetic-scale obstacles*, Physics of Plasmas 24, 022901, 2017

Acknowledgements

We thank all the LULI technical staff at École Polytechnique for their support during the experiment. The research leading to these results has received funding from the European Research Council under the European Community's Seventh Framework Programme (FP7/2007-2013) / ERC grant agreements no. 256973 and 247039, AWE plc., the Engineering and Physical Sciences Research Council (grant numbers EP/M022331/1, EP/N014472/1 and EP/N002644/1) and the Science and Technology Facilities Council of the United Kingdom. F. Cruz and L. O. Silva acknowledge support from the European Research Council (InPairs ERC-2015-AdG 695088), FCT Portugal (Grant No. PD/BD/114307/2016) the Calouste Gulbenkian Foundation and PRACE for awarding access to resource MareNostrum, based in Spain at Barcelona Supercomputing Center. The PIC simulations were performed at the IST cluster (Lisbon, Portugal), and MareNostrum (Spain). This work was supported in part at the University of Chicago by the U.S. DOE NNSA ASC through the Argonne Institute for Computing in Science under FWP 57789 and the U.S. DOE Office of Science through grant No. DE- SC0016566. The software used in this work was developed in part by the DOE NNSA ASC- and DOE Office of Science ASCR-supported Flash Center for Computational Science at the University of Chicago.

Author Contributions

G.G., B.R. A.R.B., F.F., S.L., F.M., S.S. and R.Bi. conceived this project and it was designed by G.G., S.L., and M.K. The LULI experiment was carried out by A.R., B.A., J.E.C., Y.H., P.M.K., Y.K., J.R.M., T.M., M.O., Y.S. and M.K. The paper was written by A.R., F.C., B.R. and G.G. The data was analysed by A.R. Numerical simulations were performed by F.C. and P.T. Further experimental and theoretical support was provided by R.Ba., P.G., D.Q.L., C.S., R.T. and L.O.S.

Additional Information

Supplementary information accompanies this paper at https://doi.org/10.1038/s41567-018-0059-2.

Reprints and permissions information is available at www.nature.com/reprints. Correspondence and requests for materials should be addressed to A.R.

Publisher's note: Springer Nature remains neutral with regard to jurisdictional claims in published maps and institutional affiliations.